An International Journal of Optimization and Control: Theories & Applications
ISSN: 2146-0957 eISSN: 2146-5703
Vol. 16, No. 3, pp.1126-1141 (2026)
https://doi.org/10.36922/IJOCTA026110039

RESEARCH ARTICLE

Design of adapted induction motors for variable-capacity ventilation systems

Markhabat Sakitzhanov[1*], Viktor Petrushyn[2], Nurgul Almuratova[1], Kakimzhan Gali[1], and Juriy Plotkin[3]

[1] Department of Electrical Power Engineering, Institute of Energy and Green Technologies, Almaty University of Power Engineering and Telecommunications, Almaty, Kazakhstan
[2] Department of Electromechanical Engineering, Institute of Electrical Engineering and Electromechanics, Odessa Polytechnic National University, Odessa, Ukraine
[3] Department of Electrical Engineering, Faculty of Cooperative Studies, Berlin School of Economics and Law, Berlin, Germany
m.sakitzhanov@aues.kz; victor_petrushin@ukr.net; n.almuratova@aues.kz; g.kakimzhan@aues.kz; juriy.plotkin@hwr-berlin.de

ARTICLE INFO

Article history:
Received: March 12, 2026
Revised: April 21, 2026
Accepted: April 27, 2026
Published Online: May 25, 2026

Keywords:
Adjustable-speed induction motor drive
Ventilation system
MATLAB/Simulink modeling
Dimas*Drive* software
Adapted induction motor
Discounted cost criterion

AMS Classification 2010:
93A30, 93C10, 90C30

ABSTRACT

The aim of this study is to develop an energy-efficient design approach for adjustable-speed induction motor drives used in variable-capacity ventilation systems. For such applications, the use of induction motors tailored to specific operating conditions is essential. Motor optimization based on an efficiency criterion was performed using the DIMAS*Drive* software (a specialized induction motor design tool), and the complete drive system was modeled in the MATLAB/Simulink environment. Based on the optimization and simulation results, a novel discounted cost criterion evaluated over the full operating speed range of variable-capacity ventilation loads is proposed. The criterion accounts not only for capital costs and energy efficiency, but also for the costs of reactive power and distortion power compensation, thereby reflecting both the energy performance and electromagnetic compatibility of the drive with the supply network—aspects not explicitly addressed in previously reported criteria. Structural and parametric optimization based on the proposed criterion resulted in a 19.5% reduction in the criterion value compared to a design optimized solely by the efficiency criterion, demonstrating the effectiveness and practical relevance of the proposed approach for energy-efficient drive design in ventilation applications.

1. Introduction

Variable-capacity ventilation applications are increasingly transitioning from fixed-speed to adjustable-speed drive configurations, which offer substantial reductions in electricity consumption while maintaining the required process conditions.[1–4]

When operated over a variable-speed range, standard general-purpose induction motors (IMs) exhibit suboptimal performance in power density, economic efficiency, and energy characteristics. It is therefore preferable to use specially designed adjustable-speed induction motors (ASIMs) tailored to specific operating conditions.[5–9] Spe-

* Corresponding Author

cially designed ASIMs are developed by adapting standard general-purpose IMs to the specific operating conditions of the target application in adjustable-speed drives, resulting in superior energy performance compared to non-adapted motors. The adaptation is carried out through structural and parametric optimization with respect to appropriate objective functions, the most widely used of which is efficiency, the primary indicator of energy performance.

The design of an ASIM should begin with the selection of an appropriate baseline IM, typically a standard production motor, which is then adapted for the target application. The fan is represented by the fan load characteristic, that is, by the dependence of the resisting torque on the motor-shaft speed within the specified operating range.

In addition to the conventional efficiency criterion, the design of an ASIM may also be evaluated using an innovative discounted cost criterion (DCC). This criterion considers not only the cost and energy efficiency of the ASIM drive, but also the costs associated with reactive-power compensation and distortion-power compensation. The reactive-power and distortion-power compensation components reflect both the drive's energy performance and its electromagnetic compatibility with the supply network.[10–12]

The DCC provides a comprehensive monetary assessment of drive quality. However, in its current form, this criterion does not account for the cost component associated with distortion-power compensation, leading to an underestimation of the criterion value. A method for calculating this component and incorporating it into the DCC is therefore required.

Because ventilation systems operate under specific load conditions, the selected criteria should be range-based and should account for the operating mode of the fan.[13,14]

Optimization-based design can be carried out using computer-aided tools. In this study, ASIM drive configurations based on different IMs are modeled in MATLAB/Simulink[15–19] and in the DIMAS*Drive* software package. DIMAS*Drive* includes optimization procedures that enable the development of modified ASIMs by varying the structural parameters adopted as design variables within the accepted drive configuration.

The most widely used converters in such systems are two-level transistor frequency converters with autonomous voltage inverters. The ASIM drives considered in this study are analyzed under the proportional control law U/f=const.

The advantages of adapted ASIMs over baseline IMs can be achieved by selecting an optimal combination of non-standard voltage and frequency ratings for the designed motor, coordinated with the converter's nominal parameters, while eliminating constraints on starting performance.

2. Description of the fan load characteristic

The main characteristic of a ventilation fan is the relationship between the developed total pressure H and the flow rate Q. Because these quantities are also specified for different rotational speeds (**Figure 1**), they can be used to construct the fan load characteristic for the ASIM drive. In addition, the fan efficiency values at each rotational speed must be accounted for when determining the shaft power.

The load power is determined by the following expression:

$$P = \frac{Q \cdot H}{\eta_{fan}} \cdot 10^{-3} \tag{1}$$

where Q is the fan flow rate, m^3/s; H is the total pressure, Pa; and η is the fan efficiency.

The power is also expressed as $P = M \cdot \frac{\pi \cdot n}{30}$. For known rotational speeds, the corresponding load torque values on the motor shaft can be determined. This procedure enables the transition from the H and Q relationships under speed control to the construction of the load characteristic *n(M)* (**Table 1**).

During speed control, the ventilation system output decreases from the maximum value, Q_{max}, to the minimum value, Q_{min}. The specified flow-rate range is Q_{max} = *5.48* m^3/s and Q_{min} = *1.43* m^3/s, which corresponds to a fan speed range from n_{max} = *2,300 rpm to* n_{min} = *600 rpm.* Over the same interval, the total pressure changes from H_{max} = *1,247 Pa* to H_{min}=*408 Pa.*

When designing an IM for an ASIM drive, the motor and the load must be considered together. Therefore, the comprehensive mathematical model of the drive should also include a mathematical model of the load. The mechanical load acting on the motor shaft is described by the dependence of the resisting torque on angular speed. In the general case, this relationship can be written as follows:

$$M(\omega) = M_0 + k \cdot \omega^i \tag{2}$$

where M_0 is the initial torque, N·m; k is the proportionality coefficient; ω is the angular speed of the motor shaft, s^{-1}; and i is the exponent that determines the shape of the load characteristic. Thus, the load torque at a given angular speed depends on three parameters: M_0, k, and i. These

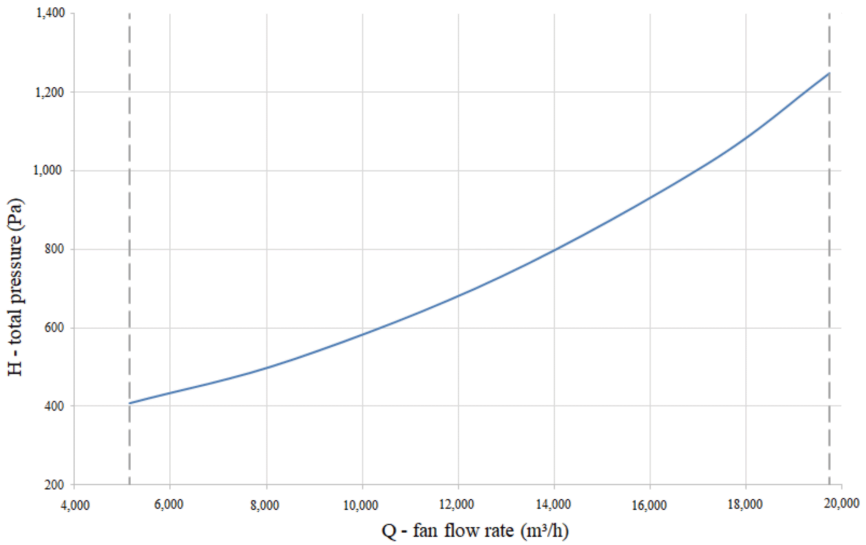

Figure 1. Total pressure–flow rate characteristic of the axial fan

Table 1. Transition from the *H=f(Q)* characteristic to the *n=f(M)* load characteristic

n, rpm	**Q, m^3/s**	**Q, m^3/h**	**H, Pa**	η_{fan}	**P, kW**	**M, N·m**
600	1.43	5,148	408	0.443	1.3	21
1,000	2.38	8,568	520	0.446	2.8	26.5
1,500	3.58	12,888	730	0.45	5.8	37
2,000	4.77	17,172	1,016	0.454	10.7	51
2,300	5.48	19,728	1,247	0.458	14.9	62

Abbreviations: H: Total pressure; M: Fan load torque; n: Rotational speed; Q: Fan flow rate–fan efficiency; P: Fan power.

parameters are chosen to ensure that the mathematical expression adequately describes the fan's actual load characteristic.

For centrifugal fan loads, the exponent usually lies in the range $i = (2...3)$. Similar characteristics are also observed for blowers, centrifugal fans, and exhausters. In this study, the fan load torque is assumed to follow a quadratic dependence on rotational speed with a certain initial torque M_0:

$$M = M_0 + k \cdot n^2 \tag{3}$$

To obtain preliminary values of M_0 and k for the load characteristic given above, a system of equations is solved:

$$\begin{cases} n_1^2 \cdot x_1 + x_2 = M_1 \\ n_2^2 \cdot x_1 + x_2 = M_2 \end{cases} \tag{4}$$

where $x_1 = k$ and $x_2 = M_0$. Using the extreme points of the speed-control range, $n_1 = 600\ rpm$, $M_1 = 21\ N \cdot m$, $n_2 = 2,300\ rpm$, $M_2 = 62\ N \cdot m$, the proportionality coefficient k and the initial torque M_0 can be determined. In matrix form, the system can be written as follows:

$$\begin{vmatrix} k \\ M_0 \end{vmatrix} = \begin{vmatrix} n_1^2\ 1 \\ n_2^2\ 1 \end{vmatrix}^{-1} \cdot \begin{vmatrix} M_1 \\ M_2 \end{vmatrix} \tag{5}$$

The solution yields the coefficient $k = 0.0083 \cdot 10^{-3}$, $M_0 = 18.1\ N \cdot m$. The resulting dependence of load torque on fan rotational speed can therefore be written as follows:

$$M = 18.1 + 0.0083 \cdot 10^{-3} \cdot n^2 \tag{6}$$

Thus, by adjusting the parameters M_0, k, and i the fan load characteristic can be approximated with the required accuracy.

3. Modeling of the adjustable-speed induction motor drive using DIMAS*Drive*

DIMAS*Drive* enables the simulation of an ASIM drive using mathematical models of its components. The drive systems considered here use identical frequency converters and operate with the same fan load. The configurations differ only in the motor type: the baseline 4A160M2 and two of its modified ASIM versions.

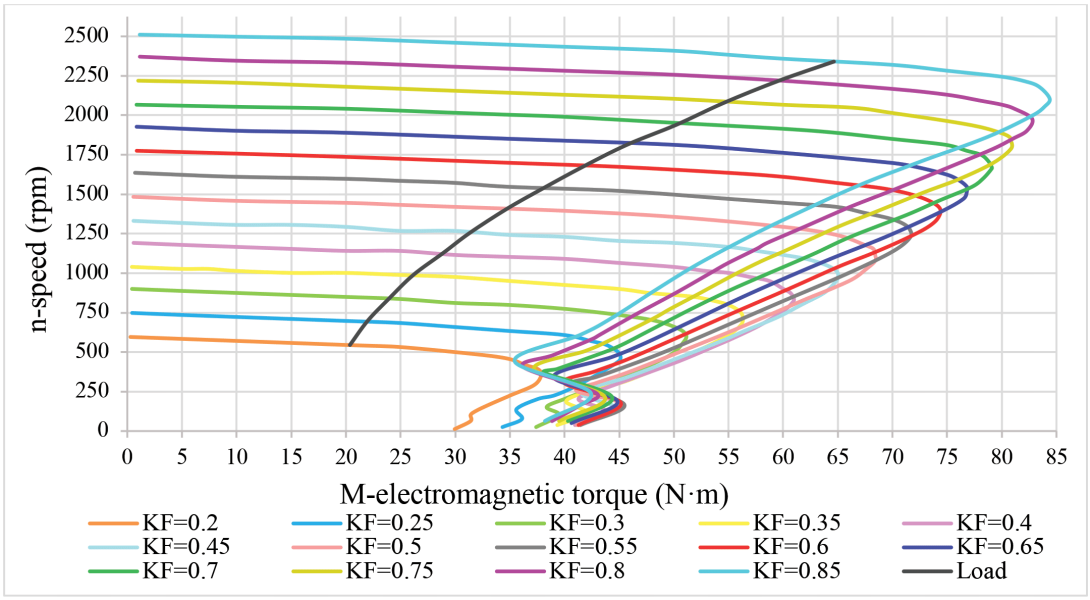

Figure 2. Family of mechanical characteristics of the induction motor 4A160M2 and the fan load characteristic

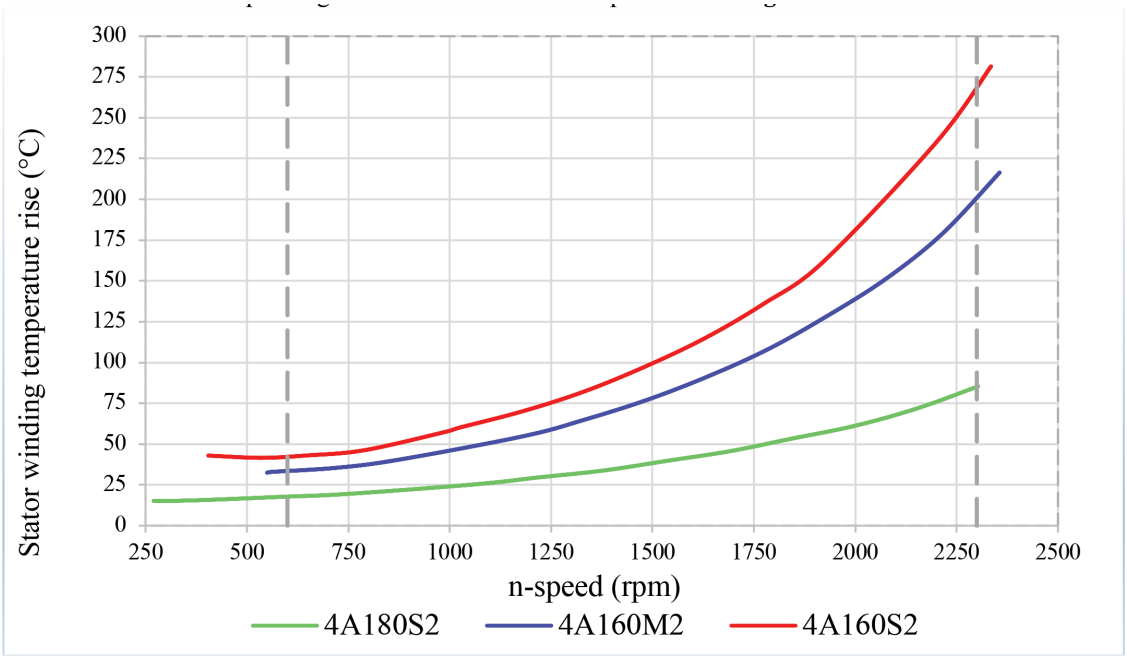

Figure 3. Thermal characteristics of the proposed induction motors

For each drive configuration, a family of mechanical characteristics can be constructed together with the superimposed fan load characteristic. The characteristics obtained for the configuration with the baseline 4A160M2 are shown in **Figure 2**.

Based on the thermal-state analysis, in particular the steady-state temperature of the stator phase winding, which is the most thermally stressed motor element, several candidate baseline motors were analyzed in DIMAS*Drive*. The corresponding thermal characteristics are presented in **Figure 3**.

Based on its thermal characteristics, the 4A160M2 motor (18.5 kW) is the most suitable baseline motor for adaptation to the fan operating conditions considered in this study. The 4A180S2 motor (22 kW) operates under a partial load, whereas the 4A160S2 motor (15 kW) and the 4A160M2 motor operate in an overloaded condition at the upper end of the control range, as indicated by the elevated temperature of the stator phase winding (**Figure 3**). Its overload is eliminated through the structural and parametric optimization procedure described in the following section.

4. Optimization-based design in the DIMAS*Drive* environment using the motor efficiency criterion

A systems-level perspective requires the simultaneous treatment of the converter, motor, and load—and, where applicable, the gearbox and supply transformer—as a unified electromechanical system. Therefore, a key feature of ASIM design is the need to use a comprehensive mathematical model of the entire drive rather than a model of the motor alone, as is commonly done for general-purpose IMs. Although modern optimization-based design methods for alternating current electrical machines are well developed, they are mainly intended for conventional machines and are not specifically focused on adapted IMs. Further improvement of mathematical and software tools is therefore required for the effective design of specialized ASIMs. In the optimization-based design of ASIMs, a range-based efficiency criterion can be applied. In this case, the motor energy performance is evaluated using a range-based criterion defined by the range-averaged efficiency over the operating speed range:

$$\eta_{avg} = \frac{1}{n_2 - n_1} \cdot \int_{n_1}^{n_2} \eta\left(n_i\right) dn \tag{7}$$

Several modifications of the baseline 4A160M2 motor are proposed. In the first modification, thin cold-rolled isotropic electrical steel grade 2211 is replaced with electrical steel grade 2411. This modification represents a structural optimization of the motor. The specific core losses of steel grade 2211 are p = 2.2 W/kg, whereas for steel grade 2411 they are p = 1.3 W/kg. In the second modification, the design obtained after the first stage is used as the initial configuration, and the stator-winding parameters, the core length, and the geometry of the stator and rotor tooth regions are optimized using the Nelder–Mead simplex method. This stage corresponds to parametric optimization of the motor design.

Table 3 presents the range-averaged efficiency values of the baseline motor and the three considered modifications over the fan speed range from $n_{min} = 600\ rpm$ to $n_{max} = 2,300\ rpm$.

Figure 4 shows the stator and rotor slot geometries of the considered motors.

In the third modification, the motor obtained in the second stage is used as the initial configuration, and the optimization procedure is repeated to further refine the stator-winding parameters, the core length L, the geometrical parameters of the stator slot region (slot height H1 and slot width GP), and the rotor geometry (distance between the circle centers A2, diameter of the larger circle D1, and diameter of the smaller circle D2).

The values of the design variables obtained from optimization in DIMAS*Drive* using the range-averaged efficiency criterion are presented in **Table 2**.

In some cases, the motor-efficiency criterion must account for the operating time at each specified rotational speed within the control range. This depends on the technological requirements of the driven mechanism. In such cases, a load time diagram, that is, a tachogram, is specified. The range-efficiency criterion of the motor is then calculated by considering the operating duration at each point of the control range according to the following expression:

$$\eta_{tg} = \frac{\sum_i \left(\eta\left(n_i\right) \cdot t_{n_i}\right.}{\sum_i t_{n_i}} \tag{8}$$

where t_{n_i} is the operating time of the motor at the rotational speed n_i, and i is the index of the tachogram segment.

If the drive operates according to the following tachogram—1 h at 600 rpm, 1 h at 1,000 rpm, and 1 h at 2,300 rpm—the values of the range-averaged efficiency criterion are those given in **Table 4**.

The dependence of motor efficiency variation within the control range is shown in **Figure 5**.

The thermal behavior of the considered modifications is significantly improved, as shown in **Figure 6**

Thus, for the considered drive system, it is preferable to use modified versions of the 4A160M2 motor rather than the baseline 4A180S2 motor, as this choice provides better size, weight, and cost characteristics.

5. Modeling in MATLAB/Simulink

The MATLAB/Simulink environment is employed as a simulation platform to evaluate the energy-performance indicators at the input of the induction motor and the drive system, including efficiency (η), phase displacement factor ($\cos\varphi$), and power coefficient (χ). The fundamental harmonic power components are determined, namely the apparent power S_1 (kVA), active power P_1 (kW), and reactive power Q_1 (kVAr). In addition, the total power components for all considered harmonics are evaluated, including the apparent power S (kVA), active power P (kW), and non-active power D (kVAr).

The non-active power D consists of two components, Q_1 and T, where Q_1 is associated with the

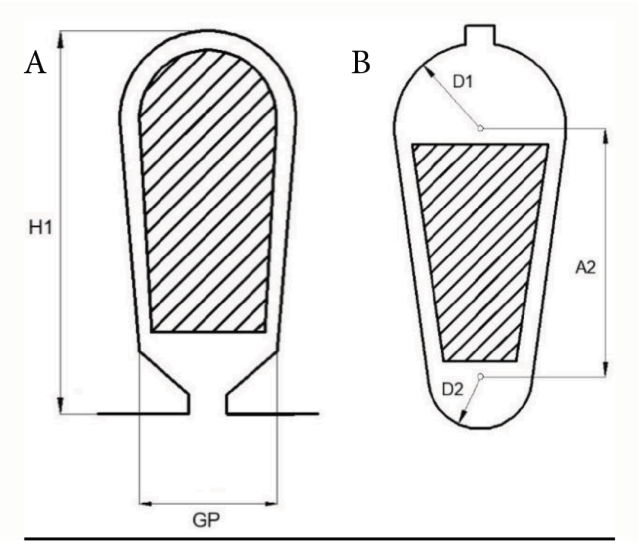

Figure 4. Stator (A) and rotor (B) slot geometries for the motors considered

Table 2. Design variables of the baseline and modified induction motors

Design variables	W_{OS}	q_{ef} mm^2	d_{ins} mm	L mm	H1 mm	GP mm	ZR	A2 mm	D1 mm	D2 mm
Baseline induction motor 4A160M2	84	2.74	1.4	130	21	11.9	28	22	7	4.9
Modification 2	65	5.64	1.97	154	28.5	13.9	31	19.9	8.3	4.7
Modification 3	57	6.61	2.11	183	29.4	13.9	30	23.5	8.3	4.6

Abbreviations: A2: Distance between the circle centers; D1: Diameter of the larger circle; D2: Diameter of the smaller circle; d_{ins} : Insulation thickness; GP: Stator slot width; H1: Stator slot height; L: Core length; q_{ef}: Effective conductor cross-sectional area; W_{OS}: Number of stator winding turns; ZR: Number of rotor slots.

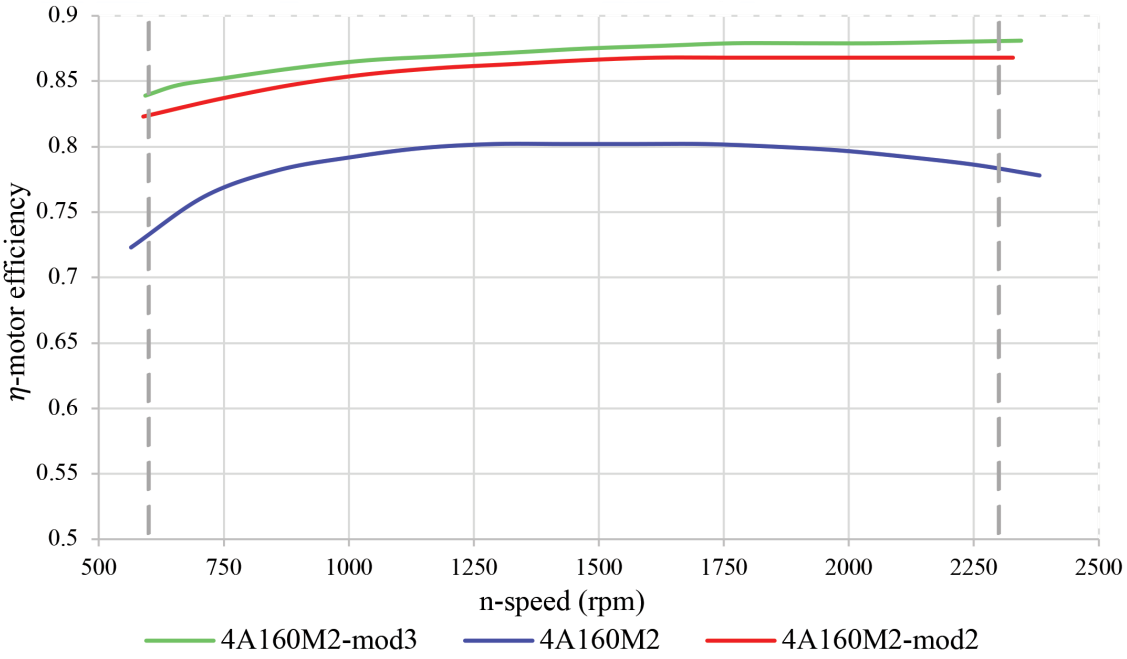

Figure 5. Motor efficiency versus rotor speed in the control range for the baseline motor and its modifications

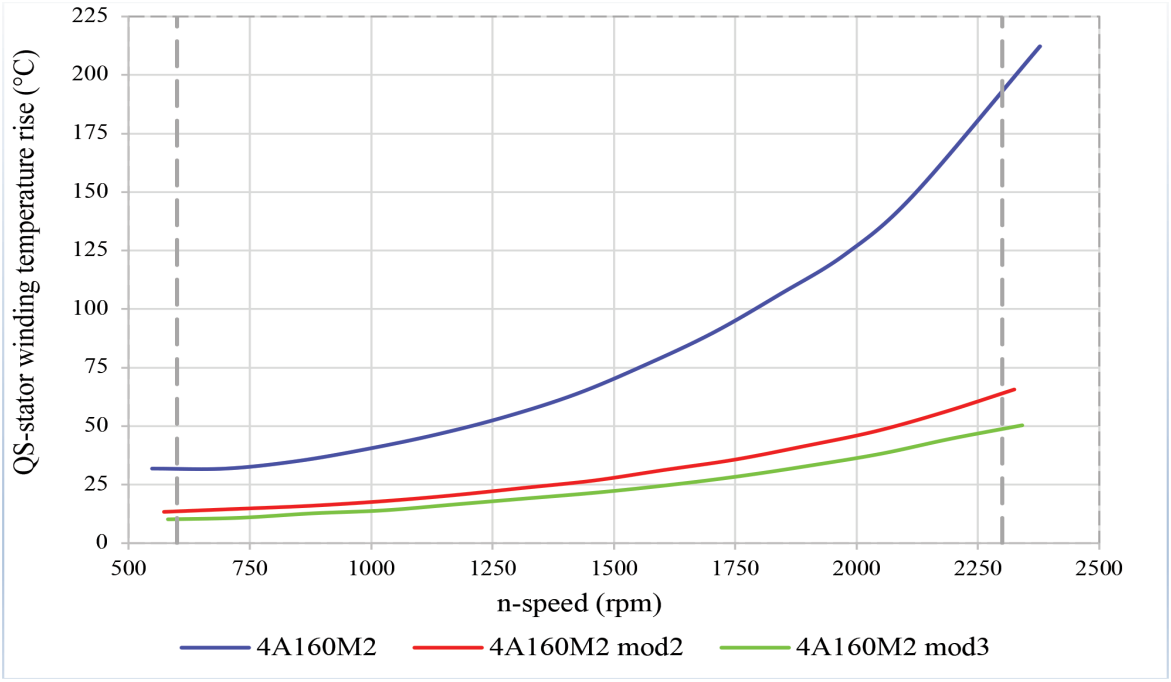

Figure 6. Thermal characteristics of the baseline induction motors and their modified designs

Table 3. Range-averaged efficiency values of the induction motors

Baseline induction motor 4A160M2	$\eta_{avg} = 0.793$
Modification 1	$\eta_{avg} = 0.814$
Modification 2	$\eta_{avg} = 0.873$
Modification 3	$\eta_{avg} = 0.883$

Table 4. Range-averaged efficiency of the baseline motor and its modifications, considering the tachogram

Baseline induction motor 4A160M2	$\eta_{tg} = 0.771$
Modification 1	$\eta_{tg} = 0.795$
Modification 2	$\eta_{tg} = 0.863$
Modification 3	$\eta_{tg} = 0.875$

phase shift between the fundamental components of current and voltage, and T represents the distortion power caused by higher harmonics. These components are related by $D^2 = Q_1^2 + T^2$. The model of the ASIM drive based on a two-stage frequency converter in the MATLAB/Simulink environment is shown in **Figure 7**. The model includes seven main functional blocks. The first block represents an ideal three-phase power supply with a line voltage of 380 V and a frequency of 50 Hz. The three-phase voltage is converted using a three-phase diode bridge rectifier. A voltage-source inverter, together with a pulse width modulation (PWM) generator, produces an output voltage at a specified frequency. The capacitance of each capacitor in the DC link is C_f =5.7 mF. The PWM carrier frequency is 6 kHz. The drive is controlled using a constant-voltage-to-frequency law, U/f = const.

The drive is loaded by a two-pole squirrel-cage IM with the following specifications: rated power P_n = 18.5 kW, rated line voltage U_n = 380 V, and rated frequency f_n = 50 Hz.

The stator parameters, including the stator resistance and stator leakage inductance, are R_s = 0.365 Ω, and L_{ls} = 2.13 mH, respectively. The corresponding rotor parameters are R_r = 0.18 Ω, and L_{lr} = 2.45 mH. The mutual inductance is L_m = 121.02 mH. The load torque characteristic is given by $M(\omega) = 18.1 + 0.757 \cdot 10^{-3} \cdot \omega^2$.

In the simulation, the load type is selected according to the specific application of the drive and may vary in magnitude and type. The system of differential equations is solved using the "discrete (no continuous states)" method with a variable time step. A time step of 2 μs is used for the calculations. The motor speed is controlled within the range of 600–2,300 rpm by adjusting the converter output frequency from 10 to 40 Hz.

In the MATLAB/Simulink simulations, measurement blocks were used to acquire instantaneous voltage and current signals from sensors, as described.[20–23]

The calculated power values enable evaluation of key performance indicators at the motor and drive system inputs, including efficiency, dis-

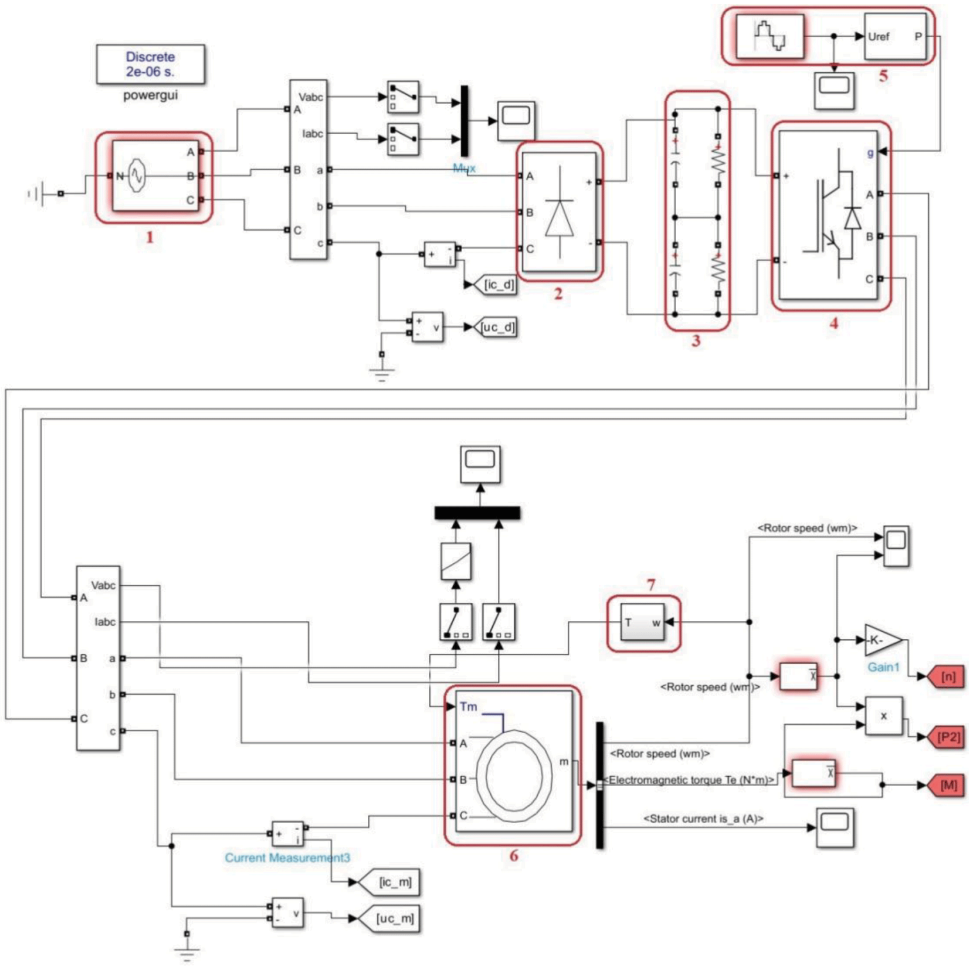

Figure 7. Simulation model of the adjustable-speed induction motor drive with a two-stage frequency converter.1: Three-phase voltage source; 2: Rectifier; 3: Direct current-link filter; 4: Voltage-source inverter; 5: Pulse width modulation generator; 6: Induction motors; 7: Load

placement power factor, total harmonic distortion (THD), and power components. Based on waveform analysis, the THD factors are determined as follows:

$$THD_U = \sqrt{\sum^{\nu} \left(\frac{U_\nu}{U_1}\right)^2}, THD_I = \sqrt{\sum^{\nu} \left(\frac{I_\nu}{I_1}\right)^2} \tag{9}$$

The power factors are calculated from the harmonic spectra of voltages and currents using the methods described[24–26]:

$$\chi = \frac{cos\varphi}{\sqrt{1 + THD_U^2 + THD_I^2 + THD_U^2 \cdot THD_I^2}} \tag{10}$$

For a system supplied by an infinite bus, supplying a distorted load with an undistorted three-phase voltage, the power factor of the electric drive is calculated accordingly[27–29]:

$$\chi = \frac{cos\varphi}{\sqrt{1 + THD_I^2}} \tag{11}$$

The DIMAS*Drive* software is used to determine the parameters of the equivalent circuit. The equivalent circuit parameters of the baseline induction motor and its modified designs, used as input data for simulations. In the MATLAB/Simulink environment, the results are presented in **Table 5**.

The simulation results of the drives employing the baseline motor 4A160M2 and its two modifications in the MATLAB/Simulink environment are presented in **Tables 6,7,8**. These tables present the energy performance indicators at the drive input for the considered drive configurations, as well as the frequency converter efficiency.

Tables 6,7,8 show differences in current, power, and rotational speed (rpm). However, the energy performance indicators remain nearly identical across the simulation results for the drives with the baseline induction motor and its two modified designs.

In MATLAB/Simulink, the power factor at the drive input can be determined either from the power balance or from the THD_I and $cos\varphi$ values.

Table 5. Equivalent circuit parameters of the baseline and modified induction motor

Parameters motor	$R_s(\Omega)$	$R_r(\Omega)$	L_{1s}(mH)	L_{1r}(mH)	L_m(mH)
Baseline induction motor 4A160M2	0.365	0.18	2.13	2.45	121.02
Modification 2	0.12	0.117	1.4	1.66	28.34
Modification 3	0.096	0.093	1.18	1.59	27.29

Abbreviations: R_r : Rotor resistance; R_s : Stator resistance; L_m : Mutual inductance; L_{1r} : Rotor leakage inductance; L_{1s}: Stator leakage inductance.

Table 6. Drive input parameters for the baseline induction motor 4A160M2

f, Hz	U, V	I, A	P, kW	n, rpm	cosφ	THDi	χ	η_{FC}
10	218.3	4.4	1.6	551	0.998	1.542	0.543	0.978
15	218.3	7.0	2.6	849	0.996	1.476	0.559	0.986
20	218.3	10.9	4.1	1,140	0.995	1.403	0.577	0.977
25	218.3	15.6	6.1	1,427	0.993	1.335	0.595	0.996
30	218.3	22.0	8.9	1,709	0.989	1.26	0.615	0.996
35	218.3	31.7	13.3	2,041	0.986	1.167	0.642	0.997
40	218.3	39.4	17.0	2,256	0.983	1.105	0.659	0.996
45	218.3	51.2	22.9	2,516	0.981	1.026	0.684	0.991

Abbreviations: χ: Power factor; cosφ: Phase displacement factor; f: Converter output frequency; I: Drive input current; n: Motor rotational speed; η_{FC}: Frequency converter efficiency; P: Total active power at the drive input; THDi: Total harmonic distortion of current; U: Drive input voltage.

Table 7. Drive input parameters for the modified induction motor (modification 2)

f, Hz	U, V	I, A	P, kW	n, rpm	cosφ	THDi	χ	η_{FC}
10	218.3	4.4	1.5	573	0.997	1.544	0.542	0.968
15	218.3	7.0	2.6	870	0.996	1.476	0.559	0.969
20	218.3	10.7	4.0	1,164	0.995	1.406	0.577	0.971
25	218.3	15.4	5.9	1,456	0.993	1.338	0.594	0.989
30	218.3	21.5	8.6	1,746	0.99	1.264	0.614	0.998
35	218.3	28.9	12.0	2,030	0.987	1.191	0.635	0.997
40	218.3	40.2	17.4	2,373	0.984	1.099	0.662	0.986

Abbreviations: χ: Power factor; cosφ: Phase displacement factor; f: Converter output frequency; I: Drive input current; n: Motor rotational speed; η_{FC}: Frequency converter efficiency; P: Total active power at the drive input; THDi: Total harmonic distortion of current; U: Drive input voltage.

6. Calculation of the range-based discounted cost criterion

The choice of design criteria is crucial in the design of ASIMs. In addition to the traditional motor-efficiency criterion, an innovative DCC can be used for the drive. Building upon the criterion introduced,10 the present work extends the discounted cost formulation to incorporate, alongside capital and energy efficiency components, the monetary costs of both reactive-power and distortion-power compensation—factors that jointly govern the electromagnetic compatibility of the drive with the supply network.[10,11,30] Because of the operating characteristics of ventilation systems, these criteria are range-based and depend on the drive's operating mode.[13]

If the active power consumed by the drive, P_1, is known, the reactive power Q_1 and the distortion power T can be determined accordingly[24,31]:

$$Q_1 = P_1 \cdot tg\varphi, \quad T = P_1 \cdot \sqrt{tg^2\chi - tg^2\varphi} \quad (12)$$

Based on the control characteristic P_1=*f(n)* and the specified drive tachogram, the active power consumed by the drive is calculated either as a range-averaged value or as a range-based

Table 8. Drive input parameters for the modified induction (modification 3)

f, Hz	U, V	I, A	P, kW	n, rpm	cosφ	THDi	χ	η_{FC}
10	218.3	4.3	1.5	579	0.997	1.547	0.542	0.968
15	218.3	6.9	2.5	877	0.996	1.477	0.558	0.968
20	218.3	10.6	4.0	1,172	0.995	1.407	0.577	0.971
25	218.3	15.3	5.9	1,465	0.993	1.339	0.594	0.988
30	218.3	21.5	8.6	1,758	0.99	1.264	0.614	0.999
35	218.3	28.9	12.0	2,045	0.987	1.19	0.635	0.997
40	218.3	40.3	17.5	2,393	0.984	1.098	0.662	0.986

Abbreviations: χ: Power factor; cosφ: Phase displacement factor; f: Converter output frequency; I: Drive input current; n: Motor rotational speed; η_{FC}: Frequency converter efficiency; P: Total active power at the drive input; THDi: Total harmonic distortion of current; U: Drive input voltage.

value weighted by the tachogram:

$$P_{1avg} = \frac{1}{n_2 - n_1} \cdot \int_{n_1}^{n_2} P_1(n_i)\, dn \tag{13}$$

$$P_{1tg} = \frac{\sum_i (P_1(n_i) \cdot t_{n_i}}{\sum_i t_{n_i}}. \tag{14}$$

Using the corresponding control characteristics, the required energy-performance indicators can be determined either as range-averaged values:

$$\eta_{avg} = \frac{1}{n_2 - n_1} \cdot \int_{n_1}^{n_2} \eta(n_i)\, dn \tag{15}$$

$$\chi_{avg} = \frac{1}{n_2 - n_1} \cdot \int_{n_1}^{n_2} \chi(n_i)\, dn \tag{16}$$

$$cos\varphi_{avg} = \frac{1}{n_2 - n_1} \cdot \int_{n_1}^{n_2} cos\varphi(n_i)\, dn \tag{17}$$

or as range-based values weighted by the tachogram:

$$\eta_{tg} = \frac{\sum_i (\eta(n_i) \cdot t_{n_i}}{\sum_i t_{n_i}} \tag{18}$$

$$\chi_{tg} = \frac{\sum_i (\chi(n_i) \cdot t_{n_i}}{\sum_i t_{n_i}} \tag{19}$$

$$cos\varphi_{tg} = \frac{\sum_i (cos\varphi(n_i) \cdot t_{n_i}}{\sum_i t_{n_i}} \tag{20}$$

The drive DCC, which can likewise be evaluated either as a range-averaged quantity or as a range-based quantity weighted by the tachogram, is calculated using the following expressions:

$$DCC_{avg} = \frac{1}{n_2 - n_1} \cdot \int_{n_1}^{n_2} DCC(n_i)\, dn \tag{21}$$

$$DCC_{tg} = \frac{\sum_i (DCC(n_i) \cdot t_{n_i}}{\sum_i t_{n_i}} \tag{22}$$

If the total cost of the drive, *CED*, is known, the DCC at a given operating point of the control range can be written as follows:

$$DCC = (CED + C_{rpc1} + C_{rpc2}) \cdot [1 + (k_d + k_s)] + C_L \tag{23}$$

where C_{rpc1} is the cost associated with reactive-power compensation, c.u.; C_{rpc2} is a novel component representing the cost of distortion-power compensation, c.u., introduced in this study; C_L is the cost of annual energy losses, c.u.; k_d is the share of depreciation costs; and k_s is the share of maintenance and operating costs. For the ASIM drive, k_d = 0.065 and k_s=0.069 are assumed, the same values used for general-purpose IMs.

If the load-time diagram of drive operation is known, that is, if the drive tachogram is specified, the expressions for C_{rpc1} and C_{rpc2} take the following form:

$$C_{rpc1}{=}c_{k1} \cdot k_{my} \cdot P_{1tg} \left[tg\left(arccos\varphi_{tg} - tg\varphi_0\right)\right] \cdot t_{ED} \tag{24}$$

where c_{k1} is the unit cost of installing 1 kVAr of reactive-power compensation equipment (10 c.u. is used in the calculations); k_{my} is the participation factor of the ASIM drive in the maximum load demand (0.25 is used in the calculations); and φ_0 is the phase angle between current and voltage at which reactive-power compensation is not required ($tg\ \varphi_0 = 0.484$ is assumed in the calculations).

The newly proposed component C_{rpc2} makes it possible to account for the cost of distortion-power compensation in accordance with the electromagnetic-compatibility requirements determined by THD:

Table 9. Performance indicators of the drive with the baseline 4A160M2

Drive Parameters	Range Is set	Tachogram Is set	Range Is set taking into account inflation	Tachogram Is set taking into account inflation
η	0.784	0.762	0.784	0.762
CED,c.u.	4,800	4,800	4,800	4,800
cosφ	0.99	0.992	0.99	0.992
P_1, kW	9.57	7.375	9.57	7.375
χ	0.609	0.591	0.609	0.591
C_{rpc2}, c.u.	57,143	46,425	57,143	46,425
C_L, c.u.	4,898	4,100	4898	4,100
K, c.u.	61,943	51,225	61,943	51,225
Y, c.u.	13,198	10,964	14,016	11,644
DCC, c.u.	75,142	62,189	75,960	62,869

Abbreviations: *CED*: Drive cost; C_L: Cost of active-power losses; cosφ: Phase displacement factor; C_{rpc2}: Cost of distortion-power compensation; DCC: Discounted costs criterion; K: Capital investment; P_1: Active power consumed by the drive; Y: Annual operating cost; η: Drive efficiency; χ: Power factor.

$$C_{rpc2} = c_{k2} \cdot k_{my} \cdot P_{1tg} \cdot \left\{ \sqrt{[tg\,(arccos\chi_{tg})]^2 - [tg\,(arccos\varphi_{tg})]^2} - tg\,[arccos\left(\frac{1}{\sqrt{1+THD_{ID}^2+THD_{UD}^2+THD_{ID}^2 \cdot THD_{UD}^2}}\right)]\right\} \cdot t_{ED} \quad (25)$$

where c_{k2} is the unit cost of installing 1 kVAr of distortion-power compensation equipment (10 c.u. is used in the calculations).

In mechatronic systems supplied from an infinite-bus system, the supply voltage can be considered sinusoidal. Under these conditions, the THD of the voltage, THD_{UD} may be taken as zero and can therefore be omitted from the above expression. Standards[32,33] specify the permissible values of the THD of current, THD_{ID}.

If the load-time diagram of drive operation is known, the annual cost of active-power losses is determined as follows:

$$C_L = c_{ae} \cdot P_{1tg} \cdot (1 + a_r - \eta_{tg}) \cdot t_{ED} \quad (26)$$

where c_{ae} is the cost of 1 kWh of active electrical energy (1 c.u. is used in the calculations); a_r is the coefficient accounting for losses in distribution networks (0.04 is used in the calculations); and t_{ED} is the annual operating time of the drive (2,000 h is used in the calculations).

If the motor operating time diagram is not specified in advance, the range-averaged values of the discounted cost components C_{rpc1}, C_{rpc2} and C_L are calculated using η_{avg}, χ_{avg}, $cos\varphi_{avg}$, and P_{1avg}.

Given that the economic payback horizon for adjustable-speed drives typically spans 5–8 years, the DCC should incorporate inflationary effects to ensure realistic long-term cost projections.[34,35]

Therefore, the DCC of the ASIM drive can generally be written as follows:

$$DCC = K + \sum_{i=1...T_n} Y_i \quad (27)$$

where $K = cep + C_{rpc1} + C_{rpc2}$ is the initial capital investment and $Y_i = (k_d + k_s) \cdot (cep + C_{rpc1} + C_{rpc2}) + C_L$ is the annual operating cost.

If inflation is neglected, the annual cost remains constant, $Y_i = const$, and equals the first-year value Y_1 determined for the initial year of operation. To account for annual inflation, the DCC can be written as follows:

$$DCC = K + Y_i \cdot \frac{1 + (1 + d_{INF1}) + ... + \left(1 + d_{INF(T_n-1)}\right)}{T_n} \quad (28)$$

where $d_{INF1}, \ldots\ d_{INF(T_n-1)}$ are the forecast inflation rates for the respective years within the payback period T_n.

For simplicity, an average annual inflation rate d_{INF1}, over the payback period, may be assumed. In this case, the inflation coefficient is determined as follows:

$$k_{INF} = \frac{\sum_{m=0}^{T_n-1} \left(1 + \frac{d_{INF}}{100\%}\right)^m}{T_n} \quad (29)$$

where d_{INF} is the average annual inflation rate, %.

Two operating modes are considered. In the first case, the drive operates over the rotor-speed

Table 10. Performance indicators of the adjustable-speed induction motor drive with modification 2 of the baseline 4A160M2

Drive	**Range Is set**	**Tachogram Is set**	**Range Is set taking into account inflation**	**Tachogram Is set taking into account inflation**
Parameters				
η	0.858	0.841	0.858	0.841
CED,c.u.	4,900	4,900	4,900	4,900
cosφ	0.992	0.993	0.992	0.993
P_1, kW	7.466	7.017	7.466	7.017
χ	0.598	0.589	0.598	0.589
C_{rpc2}, c.u.	46,074	44,448	46,074	44,448
C_L, c.u.	2,718	2,793	2,718	2,793
K, c.u.	50,974	49,348	50,974	49,348
Y, c.u.	9,548	9,405	10,140	9,988
DCC, c.u.	60,522	58,754	61,114	59,337

Abbreviations: *CED*: Drive cost; C_L: Cost of active-power losses; cosφ: Phase displacement factor; C_{rpc2}: Cost of distortion-power compensation; DCC: Discounted costs criterion; K: Capital investment; P_1: Active power consumed by the drive; Y: Annual operating cost; η: Drive efficiency; χ: Power factor.

Table 11. Performance indicators of the adjustable-speed induction motor drive with modification 3 of the baseline 4A160M2

Drive	**Range Is set**	**Tachogram Is set**	**Range Is set taking into account inflation**	**Tachogram Is set taking into account inflation**
Parameters				
η	0.868	0.853	0.868	0.853
CED,c.u.	5,000	5,000	5,000	5,000
cosφ	0.992	0.993	0.992	0.993
P_1, kW	7.455	6.894	7.455	6.894
χ	0.597	0.587	0.597	0.587
C_{rpc2}, c.u.	46,137	43,916	46,137	43,916
C_L, c.u.	2,564	2,578	2,564	2,578
K, c.u.	51,137	48,917	51,137	48,917
Y, c.u.	9,417	9,133	10,001	9,699
DCC, c.u.	60,554	58,050	61,137	58,616

Abbreviations: *CED*: Drive cost; C_L: Cost of active-power losses; cosφ: Phase displacement factor; C_{rpc2}: Cost of distortion-power compensation; DCC: Discounted costs criterion; K: Capital investment; P_1: Active power consumed by the drive; Y: Annual operating cost; η: Drive efficiency; χ: Power factor.

range 600–2,300 rpm, and the average values of the energy-performance indicators and the active power consumed by the ASIM drive are determined for this interval. In the second case, the drive operates according to a specified tachogram (3,600 s–600 rpm, 3,600 s–1,000 rpm, 3,600 s–2,300 rpm), and the energy performance indicators and the consumed active power are calculated using the corresponding expressions. In this case, reactive power compensation can be neglected because tgφ0 is significantly less than 0.484. If the average inflation rate is assumed to be 3% and the payback period is $T_n = 5$ years, the inflation coefficient is $k_{INF} = 1.062$. In the subsequent calculations, the permissible THD is set to $THD_{ID} = 10\%$. The cost of the drive with the baseline IM 4A160M2 is assumed to be 4,800 c.u., including 4,000 c.u. for the frequency converter and 800 c.u. for the baseline motor. The calculation results are presented in **Tables 9,10,11**.

One reason for the difference between the efficiency values calculated in MATLAB/Simulink and those obtained in DIMAS*Drive* is that the MATLAB/Simulink model does not account for core losses, mechanical losses, or additional stray losses in the IM. Therefore, to properly evaluate the discounted cost criterion, it is proposed to recalculate the drive efficiency as the product

of the converter efficiency obtained from MATLAB/Simulink and the IM efficiency obtained from DIMAS*Drive*.

Similarly, the performance indicators were calculated for the ASIM drive with the second modification of the baseline motor (**Table 10**). In this case, the inflation coefficient and the permissible current THD remain the same as in the previous calculation. The cost of the drive is assumed to be 4,900 c.u., because the cost of the second modification of the baseline motor is 100 c.u. higher.

Similarly, the performance indicators were calculated for the ASIM drive with the third modification of the baseline motor (**Table 11**). In this case, the inflation coefficient and the permissible current THD also remain unchanged. The cost of the drive is assumed to be 5,000 c.u. because the third modification to the baseline motor costs 200 c.u. higher.

7. Conclusion

The overall performance of adjustable-speed ventilation drives can be comprehensively evaluated using the proposed DCC. This criterion accounts for capital cost, the cost of active power losses determined by energy efficiency, and the costs associated with reactive power and distortion power compensation. These components reflect both the drive's energy performance and its electromagnetic compatibility with the supply network. Currently, no widely accepted method exists for quantifying the electromagnetic compatibility component in monetary terms. As a result, this component may be underestimated in conventional evaluations. The present study proposes an approach for its calculation and inclusion in the discounted cost criterion.

The performance of the drive is improved through the use of ASIMs developed as modifications of baseline IMs by means of structural and parametric optimization implemented in DIMAS*Drive* using the efficiency criterion. In addition, the DCC is evaluated for each design variant through simulation in MATLAB/Simulink. The design variants are assessed against this criterion, and the optimal solution is selected as the one with the minimum discounted cost.

For modeling and subsequent optimization of the ASIM drive, the ventilation unit should be represented by the load characteristic n = f(M). Structural and parametric optimization carried out in DIMAS*Drive* increases the range-averaged efficiency of the IM. The range-averaged efficiency of the baseline motor is 79.3%, increasing to 87.3% for the second modification and 88.3% for the third. Similar trends are observed when the drive operates in accordance with the specified tachogram.

For all ASIM drive variants considered, the input power factor, displacement factor, and THDi are nearly identical. Because the displacement factor is close to unity, the cost of reactive power compensation can be neglected. Within the proposed DCC, the cost of distortion-power compensation must be explicitly included, as it determines the drive's electromagnetic compatibility with the supply network.

For the range-averaged operating mode, the proposed DCC decreases by 19.46% when the second modification is used instead of the baseline motor, and by 19.41% when the third modification is used, the latter reduction being smaller due to the higher motor cost of the third modification. Therefore, the second modification is the preferred option for this operating mode. For the operating mode defined by the tachogram, the results are different: the range-based DCC decreases by 5.52% for the second modification and by 6.66% for the third modification relative to the baseline motor. Therefore, the third modification is preferable for this operating mode.

For the adopted permissible THD_i value of 10% and the assumed installation cost of 10 c.u. per 1 kVAr of distortion-power compensation equipment, this component accounts for more than 70% of the total discounted cost criterion. When inflation is taken into account, the discounted costs increase. However, the ratio between the discounted costs of ASIM drives with optimized motors and that of the drive with the baseline motor 4A160M2 remains almost unchanged.

In general, the considered drive variants can be effectively evaluated using the proposed range-based discounted cost criterion. This criterion can therefore be applied both to the analysis of existing drives and to the design of new ASIM drives.

Acknowledgments

None.

Funding

None.

Conflict of interest

The authors declare they have no competing interests

Author contributions

Conceptualization: Viktor Petrushyn, Markhabat Sakitzhanov
Formal analysis: Viktor Petrushyn, Markhabat Sakitzhanov
Investigation: Viktor Petrushyn, Nurgul Almuratova, Kakimzhan Gali
Methodology: Viktor Petrushyn
Writing – original draft: Juriy Plotkin, Markhabat Sakitzhanov
Writing – review & editing: Viktor Petrushyn, Juriy Plotkin

Availability of data

The data supporting the findings of this study are available from the corresponding author upon reasonable request.

AI tools statement

All authors confirm that no AI tools were used in the preparation of this manuscript.

References

1. Lazarev GB. Variable-frequency electric drive of pumping and ventilation units. *Silovaya Elektronika*. 2007;(3):41-48. [in Russian].
2. Prishchepov MA. On the issue of speed control range and losses of an induction motor under fan load and parametric speed control. *Agropanorama*. 2022;3(151):29-38. https://www.doi.org/10.56619/2078-7138-2022-151-3-29-38
3. Dinolova P, Ruseva V, Dinolov O. Energy Efficiency of Induction Motor Drives: State of the Art, Analysis and Recommendations. *Energies*. 2023;16(20):7136. https://www.doi.org/10.3390/en16207136
4. Turinno S, Facta M, Cahyadi. Energy saving of variable frequency drive in dust collector fan motors in the smelting process at the steel industry. *International Journal of Power Electronics and Drive Systems*. 2025; 16(2):1399-1408. https://www.doi.org/10.11591/ijpeds.v16.i2.pp1399-1408
5. Shestakov IV, Safin NR. Assessment of the need for modification of induction motors and aspects of their control when operating with frequency converters. *Energy Safety and Energy Saving*. 2019;2(86):44-48. https://www.doi.org/10.18635/2071-2219-2019-2-44-48
6. Zakharov, A.V. *Scientific Foundations of Energy Calculation and Design of AC Electrical Machines for Mechatronic Systems*. Doctoral Dissertation, National Research University "Moscow Power Engineering Institute" (MPEI), Moscow, Russia, 2017. Available online: https://mpei.ru/diss/Lists/FilesAbstracts/223-%D0%90%D0%B2%D1%82%D0%BE%D1%80%D0%B5%D1%84%D0%B5%D1%80%D0%B0%D1%82.pdf
7. Azab M. A review of recent trends in high-efficiency induction motor drives. *Vehicles*. 2025;7(1):15. https://www.doi.org/10.3390/vehicles7010015
8. Dems M, Komeza K, Szulakowski J., Kubiak W. Increase the efficiency of an induction motor fed from inverter for low frequencies by combining design and control improvements. *Energies*. 2022;15(2):530. https://www.doi.org/10.3390/en15020530
9. Balasubramanian A, Martin F, Billah MM, Osemwinyen O, Belahcen, A. Application of surrogate optimization routine with clustering technique for optimal design of an induction motor. *Energies*. 2021;14(16):5042. https://www.doi.org/10.3390/en14165042
10. Petrushin V, Plotkin J, Almuratova N, Mustafin M, Zharkymbekova M. Discounted Costs Range Criterion Modification for Controlled Asynchronous Electric Drives. *Energies*. 2023;16(15):5704. https://www.doi.org/10.3390/en16155704
11. Petrushyn V, Plotkin J, Horoshko V, Yenoktaiev R, Yakimets A. Ranged Discounted Costs Criterion Analysis for Controlled Asynchronous Drive. *International Journal on Electrical Engineering and Informatics*. 2025; 17(1). https://www.doi.org/10.15676/ijeei.2025.17.1.7
12. Turkeri C, Kiselychnyk O. Dynamical Modelling of a Centrifugal Fan Driven by an Induction Motor and Experimental Validation. *Energies*. 2023;16(18):6658. https://www.doi.org/10.3390/en16186658
13. Petrushin V, Vodichev V, Yenoktaiev R, Plotkin J. Design Criteria and Range Limits in the Development of Controlled Induction Motors. *International Journal on Electrical Engineering and Informatics*. 2019;11(2): 451-462. https://www.doi.org/10.15676/ijeei.2019.11.2.15
14. de Almeida AT, Ferreira FJTE, Both D. Technical and economic considerations in the application of variable-speed drives with electric motor systems. *IEEE Transactions on Industry Applications*. 2005;41(1):188-199. https://www.doi.org/10.1109/TIA.2004.841022
15. German-Galkin SG MATLAB & Simulink. Design of Mechatronic Systems on a PC. Saint Petersburg: Korona-Vek, 2011.
16. Saghafinia A, Ping HW, Uddin MN, Amindoust A. Teaching simulation of an adjustable-speed induction motor drive using MATLAB in an advanced electrical machines laboratory. *Procedia – Social and Behavioral Sciences*. 2013;102:96-104. https://www.doi.org/10.1016/j.sbspro.2013.10.413
17. Oladipo F, Olowu TO, Orizu EF. Analysis of the Effect of Electric and Magnetic Loadings on the

Design Parameters of an Induction Motor and Its Performance Using MATLAB/Simulink. *International Journal of Engineering Research and Applications*. 2015; 5(3):38-43.
18. Makinde KA, Bakare MS, Akinloye BO, et al. Simulation based testing and performance investigation of induction motor drives using MATLAB/Simulink. *SN Applied Sciences*. 2023;5:73. https://www.doi.org/10.1007/s42452-023-05296-w
19. Le Roux PF, Ngwenyama MK. Static and dynamic simulation of an induction motor using MATLAB/Simulink. *Energies*. 2022;15(10):3564. https://www.doi.org/10.3390/en15103564
20. Uma G, Vijayarekha K. Modeling and simulation of VSI-fed induction motor drive in MATLAB/Simulink. Indonesian *Journal of Electrical Engineering and Computer Science*. 2017;7(2):584-595. https://www.doi.org/10.11591/ijece.v7i2.pp584-595
21. Costa A, Vilaragut M, Travieso-Torres JC, Duarte-Mermoud MA. MATLAB-Based Simulation Toolbox for the Study and Design of Induction Motor FOC Speed Drives. *Computer Applications in Engineering Education*. 2012;20(2):295-312. https://www.doi.org/10.1002/cae.20396
22. Bensalem Y, Abdelkrim MN. Modeling and simulation of induction motor based on finite element analysis. *International Journal of Power Electronics and Drive Systems*. 2016;07(4):1100-1109. https://www.doi.org/10.11591/ijpeds.v7.i4.pp1100-1109
23. Klimash S, Klimash V, Vlasevsky S. Specialized modules for studying the energy performance of electrical devices in the MATLAB environment. *Electrical Systems and Complexes*. 2017;3(36):11-16. https://www.doi.org/10.18503/2311-8318-2017-3(36)-11-16
24. Petrushyn V, Horoshko V, Plotkin J, Almuratova N, Toigozhinova Z. Power balance and power factors of distorted electrical systems and variable-speed asynchronous electric drives. *Electronics*. 2021;10(14):1676. https://www.doi.org/10.3390/electronics10141676
25. Beleiu HG, Maier V, Pavel SG, Birou I, Pică CS. Harmonics consequences on drive systems with induction motor. *Applied Sciences*. 2020;10(4):1528. https://www.doi.org/10.3390/app10041528
26. Vlahinić S, Brnobić D, Vučetić D. Measurement and analysis of harmonic distortion in power distribution systems. *Electric Power Systems Research*. 2009;79(7):1121-1126. https://www.doi.org/10.1016/j.epsr.2009.02.004
27. Firago BI, Palyavchik LB. Theory of Electric Drive. Minsk: Tekhnoperspektiva, 2007. Available: https://obuchalka.org/20241006165725/teoriya-elektroprivoda-firago-b-i-pavlyachik-l-b-2007.html. Accessed May 7, 2026
28. Arrillaga J, Watson NR. Power System Harmonics. Chichester: John Wiley & Sons, 2003. https://www.doi.org/10.1002/0470871229
29. Beleiu HG, Pavel SG, Birou IMT, et al. Effects of voltage unbalance and harmonics on drive systems with induction motor. *Electrical Engineering*. 2022. https://www.doi.org/10.1080/16583655.2022.2064670
30. Song I-H, Lhee J.H, Jeong J-W. Energy efficiency and economic analysis of variable frequency drive and variable pitch system: A case study of axial fan in hospital. *Journal of Building Engineering*. 2021. https://www.doi.org/10.1016/j.jobe.2021.103213
31. Petrushin V, Plotkin J, Yenoktaiev R, Kirilenko A, Zavolinkovsky V. Theoretical and experimental results of the efficiency of a regulated asynchronous electric drive. *Pratsi Institute of Electrodynamics of the National Academy of Sciences of Ukraine*. 2020;56:53-56.
32. International Electrotechnical Commission. IEC 61000-3-2: Electromagnetic compatibility (EMC)—Part 3-2: Limits—Limits for harmonic current emissions (equipment input current ≤16 A per phase). IEC Webstore. 2018. https://webstore.iec.ch/en/publication/28164
33. International Electrotechnical Commission. IEC 61000-3-12:2011/AMD1:2021: Electromagnetic compatibility (EMC)—Part 3-12: Limits—Limits for harmonic currents produced by equipment connected to public low-voltage systems with input current >16 A and ≤75 A per phase. IEC Webstore. 2021. https://webstore.iec.ch/en/publication/64122
34. Teitel M, Levi A, Zhao Y, Barak M, Bar-Lev E, Shmuel D. Energy saving in agricultural buildings through fan motor control by variable frequency drives. *Energy Build*. 2008;40(6):953-960. https://www.doi.org/10.1016/j.enbuild.2007.07.010
35. Al-Bassam E, Alasseri R. Measurable energy savings of installing variable frequency drives for cooling towers' fans compared to dual-speed motors. *Energy Build*. 2013; 67:261-266. https://www.doi.org/10.1016/j.enbuild.2013.07.081

Markhabat Sakitzhanov *is a Master of Technical Sciences, PhD student, and Senior Lecturer at the Department of Electric Power Engineering of the Almaty University of Energy and Telecommunications named after G. Daukeyev. His professional and research interests lie in the field of electrical machines, electric drives, renewable-energy-based systems, and the dynamic stability of power systems. He actively participates in scientific and applied research projects focused on improving the efficiency, reliability, and*

intelligent control of electric drive systems, as well as the integration of modern diagnostic and modeling technologies into power engineering practice.
https://orcid.org/0000-0002-0955-8938

Viktor Petrushyn *received his Diploma degree in "Electric machines and apparatuses" at Odessa National Polytechnic University in 1968 and his Ph.D. in 1979. Since 1987 he worked as assistant professor at the department of electrical machines Odessa Polytechnic Institute. From 1993 to 1998, he was dean of the faculty of electrification and automation industry. In 2002 he had habilitated and worked since than as a professor of electrical machines at Odessa National Polytechnic University.*
https://orcid.org/0000-0003-2659-126X

Nurgul Almuratova *graduated from the Almaty Institute of Energy and Communications with a degree in Electric Drive and Automation of Technological Complexes (2001). In 2017 she defended her doctoral dissertation on the topic: "Energy-saving electric drive of centrifugal pumps for auxiliary needs of CHP" in the specialty - 6D071800 - "Electric power industry". PhD, Area of scientific interests: Improving the energy efficiency of electric drive systems in all industries. She is the author of more than 200 scientific papers, 7 textbooks, 2 of which are recommended by the Ministry of Science and Education of the Republic of Kazakhstan. Almuratova N.K. is a full member (academician) of the International Informatization Academy.*
https://orcid.org/0000-0001-8444-9822

Kakimzhan Gali *received his Diploma degree in "Power Supply of Industrial Enterprises and Cities" from the Almaty Power Engineering Institute in 1982 and the degree of Candidate of Technical Sciences (Ph.D.) in the specialty "Electromechanics and Electrical Apparatus" in 2007. From 1997 to 2001, he worked as a Senior Lecturer at Tynyshpayev Kazakh Academy of Transport and Communications. From 2001 to 2012, he worked as a Senior Lecturer and Associate Professor at K. I. Satpayev Kazakh National Technical University. Since 2012, he has been working at Gumarbek Daukeyev Almaty University of Power Engineering and Telecommunications as an Associate Professor of the Department of Electric Power Engineering.*
https://orcid.org/0009-0007-3232-6880

Juriy Plotkin *received his Diploma degree in electrical engineering/heavy current engineering at the University of Technology Berlin in 2002 and his Ph.D. in 2009, both with honors. Industrial background is based on work at Alstom Power Conversion in Berlin as project engineer for rolling mill automation. From 2010 till 2012 he has been working as a professor of renewable energy sources at Hamburg University of Applied Sciences. Since 2012 he is a professor of electrical engineering/ energy technology at Berlin School of Economics and Law*
https://orcid.org/0000-0001-9257-5933

An International Journal of Optimization and Control: Theories & Applications (https://accscience.com/journal/ijocta)